Publishing House
AKAPIT

COMPUTER METHODS IN MATERIALS SCIENCE

Informatyka w Technologii Materiałów

Vol. 9, 2009, No. 2

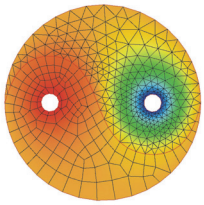

MODELLING OF MICROSTRUCTURE EVOLUTION IN HOT WORK TOOL STEELS DURING SERVICE

FRIEDRICH KRUMPHALS[1], THOMAS WLANIS[1], CHRISTOF SOMMITSCH[1], IVAN HOLZER[2], BERNHARD SONDEREGGER[2], VOLKER WIESER[3]

[1] Christian Doppler Laboratory for Materials Modelling and Simulation, Chair of Metal Forming, University of Leoben, Franz-Josef-Strasse 18, 8700 Leoben, Austria
[2] Institute for Materials Science and Welding, University of Technology, Kopernikusgasse 24, 8010 Graz, Austria
[3] Böhler Edelstahl GmbH & Co KG, Mariazellerstrasse 25, 8605 Kapfenberg, Austria
Corresponding Author: Corresponding Autor: friedrich.krumphals@mu-leoben.at (F. Krumphals)

Abstract

To establish a reliable lifetime prediction of hot work tool steels during service, it is necessary to characterize the initial microstructure as well as its evolution during application since the material properties depend on the microstructural configuration. The microstructure evolution during heat treatment is simulated with the software MatCalc, where the precipitation kinetics is of particular interest. The investigated X38CrMoV5-1 hot work tool steel, which has a bcc lattice structure, forms a distinct dislocation cell and subgrain structure, respectively, which is described by a dislocation density model for thermal creep using the rate theory with particular consideration of the subgrain boundary behaviour. The precipitation calculations with MatCalc are compared with microstructural investigations.

Key words: hot work tool steels, extrusion, microstructure modelling, dislocation density evolution

1. INTRODUCTION

Hot work tool steels are commonly in use as tools for manufacturing processes of metallic materials at elevated temperatures. Since the loading of the tools during hot metal working, e.g. extrusion, is often near the elastic limit, the lifetime is much shorter in comparison to the Cr-steels for energy applications [2]. Here, the microstructure evolution of the hot work tool steel X38CrMoV5-1 is investigated during heat treatment as well as in thermo-mechanical loading conditions, which occur during service. Therefore, the precipitation kinetics during heat treatment is calculated, using the scientific program MatCalc [3] in order to get initial conditions for a subsequent dislocation density simulation of creep loading using the rate theory with particular consideration of the subgrain boundary behaviour [1]. Subgrains as well as precipitations limit the dislocation movement and their diameter is a key parameter in determining the creep rate under varying conditions. Two different load cases, representing die loading during both, aluminium and copper extrusion [8], and the resulting microstructure evolution are demonstrated in this work.

2. HEAT TREATMENT SIMULATION AND COMPARISON WITH EXPERIMENTAL INVESTIGATIONS

The chemical composition of the hot work tool steel X38CrMoV5-1 is shown in table 1 and a standard heat treatment condition to achieve a hardness of about 48-50 HRC is depicted in figure 1. The

ISSN 1641-8581

hardening temperature is 1020°C, with a holding time of one hour and following annealing at 550°C and 580°C for two hours.

Table 1. *Chemical composition of BÖHLER W400 hot work tool steel.*

Grade \ weight %	C	Si	Mn	Cr	Mo	V	Fe
X38CrMoV5-1	0.38	0.20	0.25	5.00	1.30	0.45	bal.

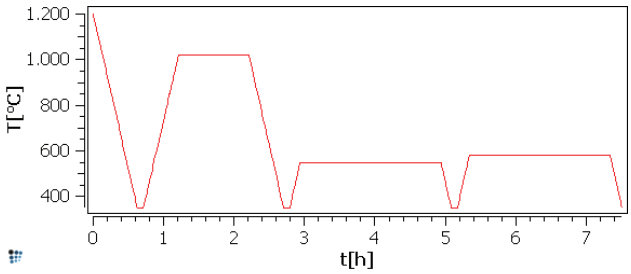

Fig. 1. *Temperature-time profile for the considered hot work tool steel X38CrMoV5-1 during heat treatment after hot working.*

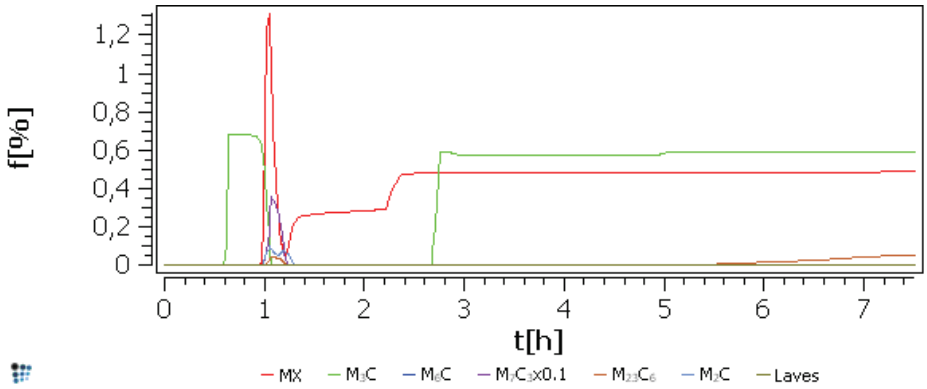

Fig. 2. *Evolution of the phase fraction of the precipitates during the heat treatment. To get a more reasonable delineation, the amount of M_7C_3 is divided by 10.*

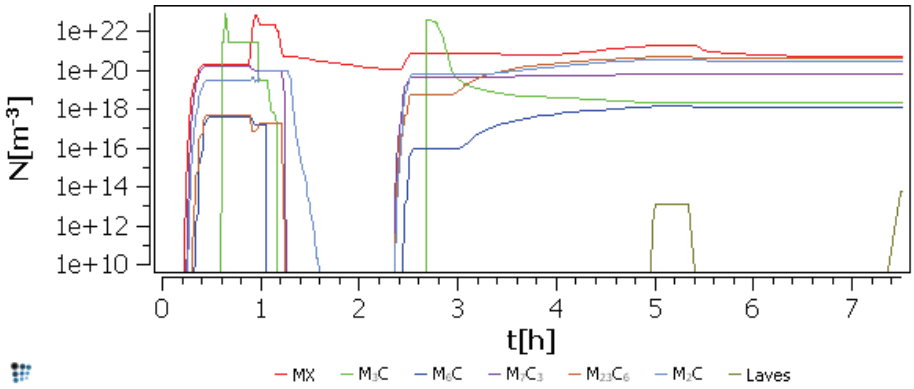

Fig. 3. *Evolution of the number of particles per volume during heat treatment.*

The temperature decrease from 1200°C at the beginning simulates the cooling from the prior hot working process. The heating up to austenitization temperature in industrial processes is performed stepwise with three hold points to assure a homogeneous temperature distribution in the billet. However, for the MatCalc simulation the exact time-temperature history of the heating up is not that important. The controlled cooling rate from austenitizing temperature is $\lambda = 8$, and after each annealing step the material is cooled by air.

The precipitation kinetics are simulated with the software MatCalc, the phase fractions f of the precipitates, namely MX (V(C,N)), M_3C (Fe_3C), M_6C (Cr_6C), M_7C_3 (Cr_7C_3), $M_{23}C_6$, ($Cr_{23}C_6$), M_2C (Mo_2C) and Laves phase are shown in figure 2, the particle number N per volume is depicted in figure 3 and the related mean radius Rv_{mean} is displayed in figure 4. Primary MX phase was not considered so far, because the phase amount was not determined quantitatively and additionally, the formation of primary phases in the liquid metal cannot be simulated in MatCalc. However, with the known primary phase fraction, the amount of dissolved carbon content in the matrix could be reduced by the amount of carbon, which has been used for the formation of the primary carbides and thus the influence of primary carbides on the precipitation kinetics of secondary carbides could be considered. Secondary phases MX, M_3C and M_7C_3 form during heating up and dissolve again during the austenitization at 1020°C. During the second annealing step, the fraction of $M_{23}C_6$ increases significantly in comparison to M_6C, M_7C_3, M_2C and Laves phase as depicted in figure 2. After the heat treatment is finished, the main existing phase fractions are M_3C, MX and $M_{23}C_6$ (M_3C: green line, MX: red line, $M_{23}C_6$ brown line in figures 2-4).

The number of particles N per volume reaches a quasi-stable condition at the end of the heat treatment, except for Laves phase (figure 3). Dislocation reactions (dipole forming, cutting, immobilizing) and precipitations have a strong influence onto dislocation structure evolution. The smaller and numerous a particle population the more it will affect dislocation glide.

M_3C precipitations are far the largest secondary particles that form during the heat treatment, which is depicted in figure 4. The significantly higher growth rate of the other secondary phases during the 30°C higher second annealing period is remarkable.

Microstructure investigations after heat treatment mainly indicated bainitic structure as well as fractions of tempered martensite. So far, only the size of M_3C carbides has been analyzed quantitatively, see figure 5. The mean radius is 75 ± 20 nm, which is in the same range as in the calculations (≈ 100 nm).

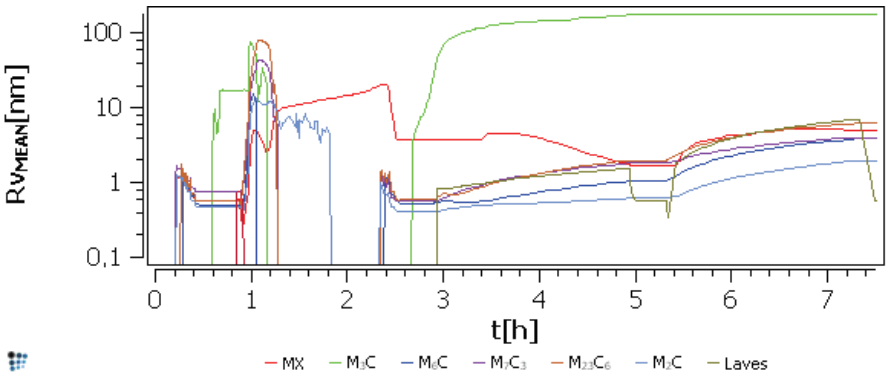

Fig. 4. *Evolution of the mean radius of the precipitates during heat treatment.*

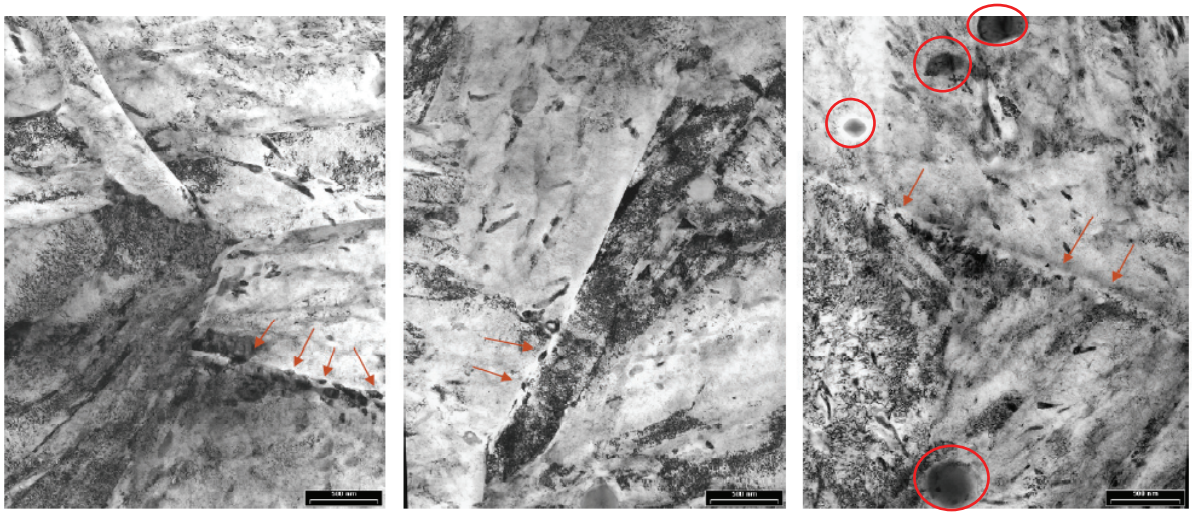

(a) **(b)** **(c)**

Fig. 5. *TEM-investigations of the bainitic microstructure show secondary precipitations at grain boundaries (M_3C, MX, marked with arrows), large primary MX carbides (marked with circles in (c)) and generally a high dislocation density. All images are 4 µm in width.*

3. MODELLING OF THE DISLOCATION STRUCTURE EVOLUTION DURING SERVICE

The precipitation state after the heat treatment, the thermal and mechanical loading conditions, the initial dislocation density as well as subgrain size are key parameters in the used physically based dislocation model according to Ghoniem et al. [1]. Since the considered thermal loads are lower than the last annealing step in the heat treatment, a constant precipitation state as initial condition is assumed and the following focus lies on the investigation of the dislocation structure.

3.1. Concept of the model

The basis of the model is to describe the dislocation structure evolution by:

- the generation and immobilization of dislocations at subgrain boundaries, i.e. multiplication as well as annihilation of dislocations due to interaction processes,
- the recovery of the static dislocations at the boundaries as well as the absorption of mobile dislocations in the cell wall,
- the generation of dislocations by emission from the cell wall,
- the dynamics of nucleation and growth of subgrains from dislocations within the cells as well as
- the subgrain growth due to coalescence driven by the subboundary energy.

Hence the total dislocation density ρ_{ges}, is separated into three categories of dislocations, namely mobile ρ_m, static ρ_s, and boundary dislocations ρ_b to consider all the specific dislocation dynamics mentioned above.

The temporal evolution of the mobile dislocation density ρ_m is given in equation 1 with v_g as the glide

velocity of the dislocations, β as a parameter for the dislocation emission, R_{sub} is the subgrain radius, h_{sg} the distance between two dislocations in the subgrain boundary, v_c^m the creep velocity of mobile dislocations and δ determines the dynamic annihilation distance: Read Frank sources Immobilization

$$\frac{d\rho_m}{dt} = \underbrace{v_g \rho_m^{0.5}}_{\text{Frank-Read-sources}} + \underbrace{\frac{\beta R_{sub}}{h_{sg}^2} v_g}_{\text{Emission from cell walls}} - \underbrace{8 v_c^m \rho_m^{3/2}}_{\text{Static recovery}} - \underbrace{\delta(\rho_m + \rho_s) v_g}_{\text{Dynamic recovery}} \quad (1)$$

The evolution equation for describing the static dislocation density is given in equation (2), where v_c^s denotes the creep velocity of static dislocations:

$$\frac{d\rho_s}{dt} = \underbrace{\frac{\rho_m}{2R_{sub}} v_g}_{\text{Immobilization}} + \underbrace{8\frac{\rho_s}{h_{sg}} v_c^s}_{\text{Static recovery}} - \underbrace{\delta \cdot \rho_s \rho_m v_g}_{\text{Dynamic recovery}} \quad (2)$$

The principle, which is valid for all three dislocation categories are dislocation generation by:
- Frank-Read sources and emission of dislocations at cell walls (ρ_m),
- immobilization (ρ_s),
- absorption and static recovery (ρ_b)

as well as the decrease of dislocation density due to:
- static and dynamic recovery (ρ_m, ρ_s),
- coalescence and growth (ρ_b).

A further important parameter, which is included in the formula of the glide velocity v_g , is the space length λ between forest dislocations. When the static dislocation density decreases, λ increases, which means easier gliding and following faster annihilation of mobile dislocations.

The effects of solutes and precipitations, which strengthen the material, are considered in the evolution of the boundary dislocation density, which can be seen in equation (3). The input parameters from the precipitation calculations $Rv_{mean,i}$ and N_i, for seven different types (i=1..7) of precipitations, which are depicted in figures 3 and 4, are introduced into the model:

$$\frac{d\rho_b}{dt} = \underbrace{8(1-2\zeta)\frac{\rho_s}{h_{sg}} v_c^s}_{\text{Absorption of dislocation and static recovery}} - \underbrace{\frac{\rho_b}{R_{sub}} M_{sg} \left[p_{sg} - 2\pi \cdot \left(\sum_{i=1}^{7} Rv_{\text{mean,i}}^2 \cdot N_i \right) \cdot \gamma_{sg} \right]}_{\text{Coalescence and growth of subgrains}} \quad (3)$$

with the parameter ζ describing the annihilation at the subgrain boundary, v_c^s the creep velocity of static dislocations, M_{sg} the mobility of subgrains, p_{sg} the driving force of the subgrain boundary, $Rv_{mean,i}$ the radius of precipitation class i, N_i the related number of particles per volume and γ_{sg} the surface energy of the subgrain boundary.

The microstructure calculations can be compared with FE-Simulations and experiments [6,8] via the resulting true inelastic strain rate $d\varepsilon/dt$, which is an additional output of the model:

$$\frac{d\varepsilon}{dt} = \frac{1}{M} \rho_m v_g b \quad (4)$$

where $M = 3$ is the Taylor factor for the bcc lattice structure [7] and b is the burgers vector.

3.2. Calculation of the dislocation density evolution during thermo-mechanical loads

During austenitization at 1020°C for one hour, the total dislocation density decreases, but during quenching bainite and martensite form, this causes high stresses and strains in the lattice structure, generating dislocations. The total dislocation density after austenitization and quenching, to produce mainly bainitic structure in our case, can be assumed to be $\rho_{ges}=10^{12}$ m^{-2}, i.e. $\rho_m= 8\cdot10^{11}$ m^{-2}, $\rho_s=1\cdot10^{11}$m^{-2} and $\rho_b=1\cdot10^{11}$ m^{-2} [10] and $R_{sub}= 7\cdot10^{-7}$ m.

The dislocation density calculations in this paper are executed for constant mechanical loads of 370MPa at 500°C (figure 6a), which should represent a heavily loaded point in the liner for aluminium extrusion application [8,9] and 750MPa at 570°C (figure 6b), which is a realistic case for copper extrusion [4, 5] and that is near the elastic limit at these conditions.

Calculations were performed with MathCad™ with the initial conditions as mentioned before and the loading time was set to 40 hours ($1.44\cdot10^5$ seconds), which equals to 500 – 2000 press cycles in typical extrusion processes, however the cyclicality of loading has been neglected so far.

The total dislocation density at a load of 370MPa and 500°C increases very slowly (figure 6a), the main mechanism is the formation of a stable subgrain structure, i.e. the dislocation density in the cell walls increases significantly whereas the mobile as well as the static dislocation density finally decreases and the subgrain size almost remains constant. The macroscopic strain after 40 hours of loading is small in comparison to the strain occurring at

the considered higher thermo-mechanical load case (figure 6b), where the dislocation structure immediately begins to change and a distinctive subgrain structure is formed. Remarkable is the resulting higher dislocation density of ρ_{ges}= $2 \cdot 10^{14}$ m^{-2} in comparison to $1.5 \cdot 10^{12}$ m^{-2} for the lower load case. The diagrams also show that a constant total dislocation density production rate (slope of blue curve in figures 6a,b) develops with progress in time.

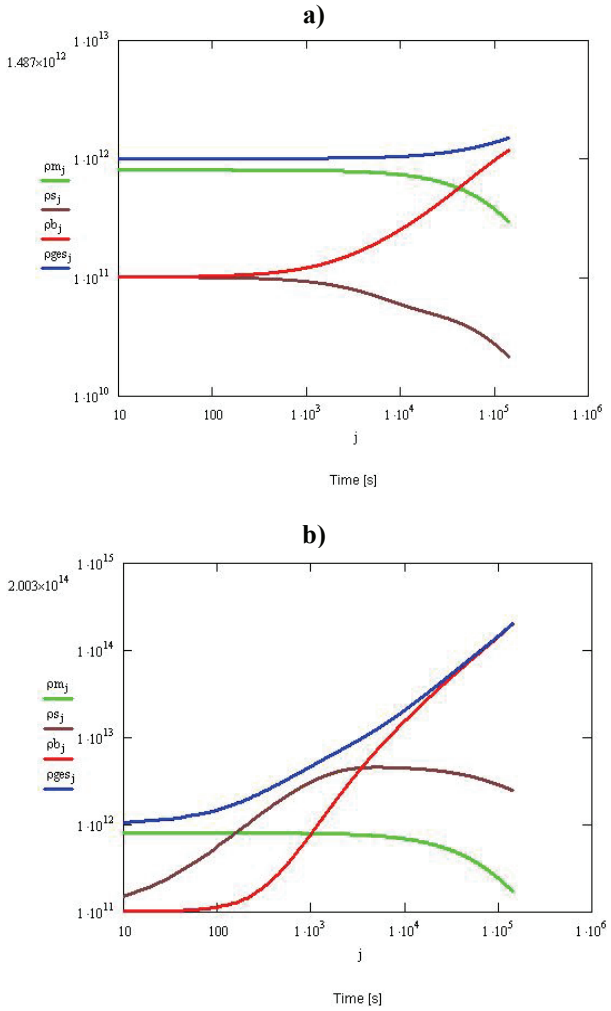

Fig. 6. *Evolution of the mobile (ρ_m, green line), static (ρ_s, brown line), boundary (ρ_b, red line) and total (ρ_{ges}, blue line) dislocation density [m^{-2}] at 500°C and 370MPa (a) and 570°C and 750MPa (b) in double logarithmic scale.*

To validate the dislocation density model, the resulting inelastic strain is compared (figure 7) with ABAQUS calculations including an elastic-viscoplastic Chaboche type constitutive model that has been validated by a comprehensive experimental program [8].

The ABAQUS simulation output for the accumulated viscoplastic strain for 370MPa at 500°C after 40 hours amounts to $2.5 \cdot 10^{-5}$, whereas the result from the microstructure model is $1.0 \cdot 10^{-4}$, which is fairly comparable, while the results for the second considered thermo-mechanical load case agree better. Remarkable is that the dislocation density model exhibits a constant slope (d log ε / d log t), contrary to the ABAQUS model results.

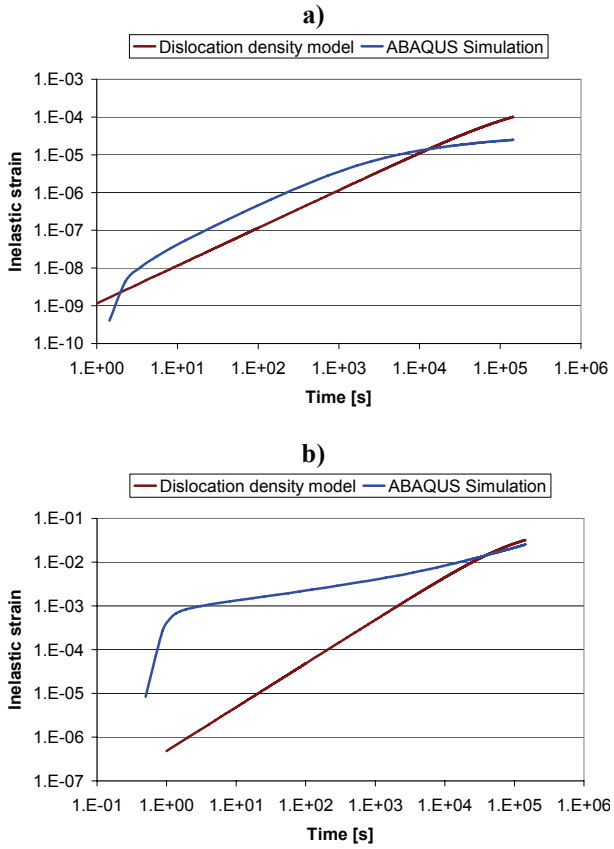

Fig. 7. *Comparison of the calculated (this work, brown curve) as well as FE-simulated ([8], blue curve) inelastic strains for 370MPa at 500°C (a) and 750MPa at 570°C (b).*

4. CONCLUSIONS AND OUTLOOK

In this work it was shown, that by applying physical based models, the microstructure evolution of hot work tool steels during both heat treatment and industrial service can be described. Precipitation of secondary phases during annealing was modelled in order to consider the significant influence of the precipitation state on the mobility of dislocations. However, possible further precipitation reactions during service, which was related to short time dislocation creep, were neglected. On the basis of two chosen examples, i.e. aluminium extrusion and copper extrusion, representative loads were applied to calculate the evolution of mobile, static and boundary dislocation densities as well as of the subgrain structure. Resulting inelastic accumulated strains were compared with the outcome of a constitutive formerly validated model.

To further validate the microstructure calculations, the secondary hardening carbides in the material will be analysed after the heat treatment as well as during service in more detail. The model for the calculation of the dislocation density and subgrain size evolution will be verified by dislocation density measurements as well as via the resulting inelastic strain, which can be compared to both macroscopically measured and viscoplastically simulated values. Additionally, damage evolution as well as lifetime estimation of hot work tool steels shall be modelled in order to make progress in both materials development and process optimization.

REFERENCES

1. Ghoniem, N., Matthews, J., Amodeo, R., A dislocation model for creep in engineering materials, Res Mechanica, 29, 1990, 197-219.
2. Holzer, I., Rajek, J., Kozeschnik, E., Cerjak, H.-H., Simulation of the precipitation kinetics during heat treatment and service of creep resistant martensitic 9-12% Cr Steel, Proc. Materials for Advanced Power Engineering, Liege, 2006, 1191-1198.
3. Kozeschnik, E., Sonderegger, B., Holzer, I., Rajek, J., Cerjak, H., Computer simulation of the precipitate evolution during industrial heat treatment of complex alloys, Materials Science Forum, 539-543, 2007, 2431-2436.
4. Krumphals, F., Wlanis, T., Sommitsch, C., Buchner, B., Huber, D., Redl, C., Wieser, V., Creep fatigue in hot work tool steels during copper extrusion, Proc. Sixth International Conference on Low Cycle Fatigue, Berlin, eds, Portella, P.D. et al., DVM Berlin, 2008, 721-726.
5. Krumphals, F., Wlanis, T., Sommitsch, C., Redl, C., Creep fatigue of multi-part container during hot extrusion of copper – Simulation and experimental comparison, Computer Methods in Materials Science, 7, 2007,47-53.
6. Mitter, W., Haberfellner, K., Danzer, R., Stickler, C., Lifetime prediction of hot work tool steels, Lab. Report, Journal of Heat Treatment and Materials Science (HTM), 52, 1997, 253-258.
7. Orlova, A., Miclicka, K., Dobes, F., Choice of evolution equation for internal stress in creep, Materials Science and Engineering, A194, 1995, 9-16.
8. Sommitsch, C., Sievert, R., Wlanis, T., Günther, B., Wieser, V., Modelling of creep-fatigue in containers during aluminium and copper extrusion, Computational Materials Science, 39, 2007, 55-64.
9. Sommitsch, C., Krumphals, F., Stotter, C., Dendl, D., Wlanis, T., Huber, D., Wieser, V., Lifetime comparison of different hot work tool steels for extrusion tools in aluminium extrusion, Proc. ET'08-Ninth International Aluminium Extrusion Technology Seminar and Exposition, Orlando, 2, 2008, 425-436.
10. Weinert, P., Modellierung des Kriechens von ferritisch/martensitischen 9-12% Cr-Stählen auf mikrostruktureller Basis, PhD thesis, University of Technology, Graz, 2001 (in German).

MODELOWANIE ROZWOJU MIKROSTRUKTURY STALI NARZĘDZIOWYCH PODCZAS OBRÓBKI CIEPLNEJ I PRACY W WARUNKACH EKSPLOATACYJNYCH

Streszczenie

Tematem pracy jest przewidywanie czasu pracy narzędzi w warunkach eksploatacyjnych. Końcowe własności wyrobu zależą od jego początkowej mikrostruktury oraz zmian tej mikrostruktury podczas wytwarzania. Dlatego za główny cel pracy postawiono sobie modelowanie rozwoju mikrostruktury podczas procesu obróbki cieplnej oraz pracy narzędzi w warunkach eksploatacyjnych. Modelowanie ewolucji mikrostruktury ze szczególnym uwzględnieniem kinetyki wydzieleń wykonano z wykorzystaniem pakietu MatCalc. W pracy analizie poddano stal narzędziową X38CrMoV5-1 o strukturze bcc, która tworzy wyraźną strukturę dyslokacyjną oraz podziarnową. Wykonane obliczenia numeryczne poddano również weryfikacji doświadczalnej.

Submitted: October 24, 2008
Submitted in a revised form: December 1, 2008
Accepted: December 18, 2008